Journal of Engineering and Sustainable Development
Vol. 30, No. 02, March 2026
https://jeasd.uomustansiriyah.edu.iq/index.php/jeasd
ISSN 2520-0917
Research Article
https://doi.org/10.31272/jeasd.2223

Behavior of Concentrically Loaded RPC Circular Columns Reinforced Longitudinally and Transversally with GFRP Bars

Mohamed Qassim Kadhim[1, *], Hassan Falah Hassan [1]

[1]Civil Engineering Department, College of Engineering, Mustansiriyah University, Baghdad, Iraq

[*]Email: mohammedkasim9244@gmail.com

Article Info

Received 02/11/2023
Revised 27/02/2026
Accepted 27/02/2026

Abstract

Although reinforced concrete (RC) members with glass fiber reinforced polymer (GFRP) bars have been widely investigated, the axial performance of reactive powder concrete (RPC) columns reinforced with GFRP has not been sufficiently addressed. To fill this gap, an experimental program was carried out on eleven circular specimens, each 150 mm in diameter and 1000 mm in height. The specimens were divided into four groups: three groups of fully GFRP-reinforced columns with hoop spacings of 40, 60, and 80 mm, and a reference group including one steel-reinforced column and one hybrid column combining steel and GFRP bars. Both reference specimens used GFRP hoops at 60 mm spacing. The study examined failure mechanisms, ultimate axial strength, deformation responses (strain and displacement), and ductility. Increasing the main reinforcement ratio from 1.77% to 3.55% enhanced axial capacity by about 46%, while raising the transverse reinforcement ratio from 1.24% to 2.48% improved load capacity by 10–19%. Higher confinement also contributed to better ductility. Although GFRP-RPC columns showed lower nominal strength compared with steel- and hybrid-reinforced RPC columns, their overall structural behavior followed similar trends. The experimental results were further used to evaluate the accuracy of existing design equations in predicting the nominal axial capacity of GFRP-RPC columns.

Keywords: Axial load; Concrete columns; Ductility; Glass fiber reinforced polymer bars; Hoops; Reactive powder concrete.

1. Introduction

Among structural components, reinforced concrete (RC) columns play a critical role in ensuring overall system stability and load transfer. The failure of a column is particularly critical, as it may trigger progressive collapse and severe structural damage [1]. Circular RC columns are widely implemented in bridge piers and foundation piles due to their geometric efficiency, aesthetic appeal, and uniform resistance to lateral actions such as wind and seismic loading [2]. Over the past several decades, fiber-reinforced polymer (FRP) materials have emerged as a viable alternative to conventional steel reinforcement. Their growing adoption is largely attributed to superior corrosion resistance and favorable mechanical properties, including high tensile strength-to-weight ratio, reduced self-weight, simplified installation, minimal maintenance requirements, and excellent durability even under aggressive environmental conditions [3]. FRP has grown in popularity as a steel replacement in RC structures. Glass fiber reinforced polymer (GFRP) bars are more prevalent in the construction industry than other types of FRPs due to their lower cost, according to the ACI 440.1R-15 guide [4]. GFRP bars are cheaper due to more competition and a broader market. GFRP bars reinforce concrete bridges, parking garages, tunnels, and water tanks [5]. The favorable mechanical and chemical characteristics of GFRP reinforcement have led to its increasing adoption in infrastructure applications [6],[7]. Continuous experimental research on FRP bars has significantly influenced the evolution of international design standards. Earlier provisions, such as CSA S806-12 [8], neglected the compressive contribution of FRP reinforcement. However, this perspective has evolved in the updated CSA S807-19 [9], where FRP bars are acknowledged as participating elements in compression members. In contrast, previous ACI recommendations—including ACI 440.1R-06 [10] and ACI 440.1R-15 [4]—discouraged the use of longitudinal FRP reinforcement in concrete compression members. More

recently, ACI 440-22 [11] has permitted the application of GFRP bars in compression elements; nevertheless, their maximum axial resistance is not explicitly accounted for in capacity calculations. The distinct behavior of GFRP under compressive loading is primarily attributed to its relatively low compressive strength compared with its tensile capacity. The combination of GFRP reinforcement with high-performance materials such as Reactive Powder Concrete (RPC) offers potential advantages. As noted in ACI 440.1R-15 [4], higher concrete compressive strength enhances composite action and compatibility between FRP bars and the surrounding matrix, particularly when both materials exhibit high strength characteristics. France invented cementitious composite RPC in the 1990s. The earliest bridge constructed using RPC was the Sherbrooke Bridge in Canada. RPC is ultra-strong and ductile. RPC's particle gradients improve microstructure and density. Use fine pozzolanic components like silica fume and adjust Portland cement's chemical characteristics to form the strongest hydrates [12]. Experimental investigations on axially loaded RPC columns reinforced with steel have demonstrated effective composite interaction between steel reinforcement and RPC at the early loading stages. Failure was typically characterized by longitudinal splitting near the column ends, with cracks propagating toward the mid-height region [13]. Parametric studies examining the influence of transverse reinforcement reported that variations in bar diameter (4, 6, and 8 mm) and spacing (100, 140, and 175 mm) significantly affected column behavior. It was observed that, in short conventional concrete columns, the diameter of transverse reinforcement played a more dominant role than spacing in enhancing confinement efficiency. Modifying the transverse bar diameter resulted in an ultimate capacity increase of up to 203%, whereas adjusting spacing led to a maximum increase of 179% [14]. Further research indicated that increasing the main reinforcement ratio, steel volumetric ratio, and lateral stirrup ratio contributed to improvements in axial compressive resistance of steel-reinforced RPC columns. Notably, higher stirrup ratios were associated with enhanced post-peak load-carrying performance [15]. In comparison with steel-reinforced counterparts, solid circular GFRP-RC columns have demonstrated superior performance in terms of load capacity, confinement effectiveness, and ductility characteristics. Experimental evidence indicates that high-strength concrete (HSC) columns reinforced with either steel or GFRP exhibit comparable structural performance under concentric axial compression, particularly prior to the introduction of load eccentricity. Nevertheless, substituting steel reinforcement with an equivalent GFRP ratio under concentric loading conditions resulted in an approximate 30% reduction in ductility. The incorporation of closely spaced spiral reinforcement was shown to mitigate this limitation by enhancing ductility and improving the after-ultimate axial load–displacement response in GFRP-reinforced HSC samples [16]. The influence of longitudinal reinforcement ratio has also been widely examined in GFRP-RC columns. Varying the enhancement ratio between 0.36% and 3.24% produced load improvements of 3.4% to 25.7%, together with a corresponding increase in ultimate strain ranging from 2.64% to 75.6%. The direct contribution of GFRP longitudinal bars to the total load capacity was reported to range from 0.72% to 6.71% [17]. Although GFRP-reinforced columns generally demonstrate behavioral trends comparable to steel-reinforced members, their nominal axial capacity tends to be slightly lower. For instance, reductions of approximately 6.7% in nominal capacity (P_n) relative to steel-RC columns have been reported, despite similar maximum load values (P_{max}). Importantly, increasing the longitudinal GFRP ratio consistently enhances nominal capacity [18]. The role of transverse reinforcement is equally significant. GFRP specimens with transverse confinement exhibited approximately 15% higher ductility but about 12.3% lower load compared with steel-reinforced counterparts. Increasing the amount of longitudinal reinforcement and reducing spiral pitch were found to improve both load resistance and deformation capacity. When adequate transverse confinement was provided, the load capacities of steel- and GFRP-reinforced columns became nearly comparable [19]. The peak load of hollow concrete columns incorporating GFRP bars and helices exhibited a slight increase, from 5% to 10%, when the reinforcement ratio was elevated from 1.89% to 3.79%. However, confinement efficiency increased substantially from 1.43 to 2.23, and the ductility factor improved markedly from 1.36 to 3.05. On average, GFRP longitudinal reinforcement contributed approximately 11% of the ultimate load capacity. Moreover, hollow GFRP-reinforced columns demonstrated superior performance compared with equivalent solid specimens [20].

A review of the existing literature reveals extensive experimental and analytical work on conventional concrete columns reinforced with either steel or FRP bars. Nevertheless, despite the growing application of reactive powder concrete (RPC) as an advanced cementitious material, the structural response of FRP-reinforced RPC columns has not yet been systematically documented. To the best of the authors' knowledge, no experimental data are currently available concerning FRP-RPC compression members. Accordingly, the current study investigates the axial behavior of circular GFRP-RPC columns by examining the influence of three primary parameters: (i) longitudinal reinforcement ratio, (ii) transverse reinforcement ratio, and (iii) the type of longitudinal reinforcement, including GFRP, conventional steel, and hybrid combinations. This investigation aims to clarify the interaction between high-performance concrete matrices and non-metallic reinforcement systems under concentric axial loading.

2. Materials and Methods

2.1 Experimental Program.

2.1.1 Concrete

The RPC mixture adopted in the current investigation was formulated with a high proportion of Portland cement serving as the binder, supplemented by silica fume as a secondary cementitious material to enhance matrix densification and mechanical performance. A finely graded quartz sand (Sikadur-504) with particle sizes ranging between 0.08 and 0.2 mm was utilized as the aggregate phase. The detailed particle size distribution of the fine aggregate is presented in Table 1 and Fig. 1, demonstrating compliance with the limits specified in Iraqi Specification No. 45/1984 [21]. Consistent with RPC

design principles, both the sand-to-cement and water-to-cement ratios were maintained at relatively low values to achieve high strength and reduced porosity. To ensure adequate workability despite the low water content, a high-range water-reducing admixture (Viscocrete-171) was incorporated at an optimized dosage to produce a highly flowable mix. The selected mix proportions were based on the formulation proposed by Hassan [22], aiming to achieve maximum compressive strength together with a flow value of 95%, as determined in accordance with ASTM C109/C109M-21 [23] and ASTM C1437-20 [24]. The RPC mixture described previously was utilized for casting all column specimens as well as the control samples, as summarized in Table 2. The concrete compressive strength was obtained by testing three concrete cylinders in compression with 100 × 200 mm dimensions according to ASTM C39/C39M-21 standard [25]. The average compressive strength of the specimens was 85 MPa. A splitting tensile test was conducted by testing three concrete cylinders with 100 × 200 mm dimensions to obtain the tensile strength of concrete according to the ASTM C496/C496M-17 standard [26], and the average splitting tensile strength was found to be 7.75 MPa.

Table 1. Grading of fine sand compared with the requirement of Iraqi specification No.45/1984 [21] *

Sieve size (mm)	Cumulative passing %	Limits of Iraqi specification No.45/1984 [21], zone 4
4.75	100	95-100
2.36	100	95-100
1.18	100	90-100
0.600	100	80-100
0.300	47	15-50
0.150	13	0-15

* This test was made at the Engineering Consultancy Bureau (E.C.B.) laboratory at the College of Engineering, Mustansiriyah University.

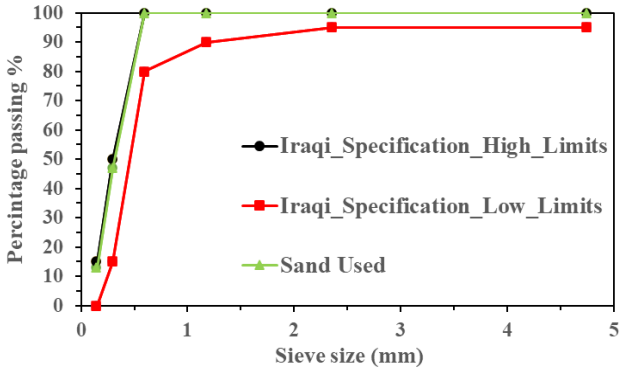

Figure 1. The grading curve of the separated sand.

Table 2. The mix proportion details of RPC

Cement K_g/m^3	Sand K_g/m^3	Silica fume % *	Silica fume K_g/m^3	W/C	Viscocrete 171 precast % *
900	900	25	225	0.18	5

* Percent of mix volume.

2.1.2 GFRP Bars.

The GFRP reinforcement employed in this study was manufactured by Nanjing Fenghui Composite Co., Ltd. and assessed according to ASTM D7205/D7205M-21 [27]. High-modulus (HM) GFRP bars, designated as No. 3 with a nominal diameter of 10 mm (Fig. 2), were used as longitudinal reinforcement for the circular column specimens. Transverse confinement was provided using No. 2 HM GFRP circular hoops with a nominal diameter of 6 mm, as shown in Fig. 3. The hoops were manufactured with a 120 mm external diameter and a 60 mm splice overlap. The GFRP bars were generated via the pultrusion process, in which E-glass fibers are impregnated with a high-durability resin. To enhance bond performance and improve load transfer between reinforcement and concrete, the bar surfaces were sand-coated. The main mechanical characteristics of the GFRP bars, as provided by the fabricator, are summarized in Table 3.

Figure 2. GFRP longitudinal reinforcement.

Figure 3. GFRP transverse reinforcement.

Table 3. Key mechanical properties of the high-modulus GFRP reinforcement used in this study *

Type No.	Bar size	Nominal Diameter (mm)	Ultimate tensile strength (MPa)	Modulus of Elasticity (GPa)	Weight (g/m)	Transverse shear strength (MPa)
B 100-6	#2	6	896	46	77.4	150
B 100-10	#3	10	827	46	159	

* Provided by the manufacturer.

2.1.3 Steel Reinforcement.

For the Steel and Hybrid columns, deformed steel bars with a nominal diameter of 10 mm were employed as longitudinal reinforcement.

The mechanical characteristics of the Grade 60 steel bars utilized are summarized in Table 4. Bar tests performed on three 10 mm specimens confirmed that the material properties conform to the requirements specified in ASTM A615/A615M-22 [28].

Table 4. Steel bar properties *

Properties	Analysis	Limits of specification requirement A615/A615M-22 [28]
Nominal Diameter (mm)	10	-
Yield stress, f_y (MPa)	466.33	≥ 420
Ultimate stress, f_u (MPa)	626.33	≥ 550
Elongation %	9.3	9 % min

* This test was made at the Engineering Consultancy Bureau (E.C.B.) laboratory at the College of Engineering, Mustansiriyah University.

2.1.4 Specimen's Details.

The research program consists of casting and testing eleven RPC circular columns divided into four groups under concentric axial compression loading. Three groups consisted of nine concrete columns that were longitudinally and transversally reinforced with GFRP bars and hoops. The remaining two columns were prepared as references within the fourth group: one reinforced with longitudinal steel bars and transverse GFRP hoops, and the other column is a hybrid (Steel and GFRP) longitudinal bars and transverse GFRP hoops. All columns were 150 mm in diameter and 1000 mm in height, with an effective length of 750 mm, and were examined. A uniform concrete cover of 15 mm was maintained from the face of the transverse hoops for all columns. The overall dimensions, reinforcement configuration, and arrangements of the tested columns are illustrated in Fig. 4. The experimental program was designed to systematically investigate the effects of volumetric enhancement ratios, longitudinal enhancement ratios, and the type of longitudinal reinforcement. Details of the test matrix and reinforcement arrangements are summarized in Table 5. Each sample was labeled using a two-part code: the initial letters (G, S, and GS) denote columns reinforced with GFRP, steel, or a hybrid combination of GFRP and steel, respectively. The second letter indicates the transverse hoop configuration, while the left number specifies the quantity of main bars, and the right number represents the spacing of the transverse reinforcement. For the control columns, transverse confinement was provided using 6 mm diameter rounded GFRP #2 hoops spaced at 60 mm.

Table 5. Detailed experimental layout and reinforcement configurations of the tested circular columns

Column's designations		Longitudinal Reinforcement			Transverse Reinforcement			
		Material type	No. & size (mm)	ρ_l%	Material type	size (mm)	Spacing (mm)	ρ_t%
G1	G4-H40	GFRP bars	4 & 10	1.77	GFRP hoops	ϕ6	40	2.48
	G6-H40		6 & 10	2.66				
	G8-H40		8 & 10	3.55				
G2	G4-H60	GFRP bars	4 & 10	1.77	GFRP hoops	ϕ6	60	1.65
	G6-H60		6 & 10	2.66				
	G8-H60		8 & 10	3.55				
G3	G4-H80	GFRP bars	4 & 10	1.77	GFRP hoops	ϕ6	80	1.24
	G6-H80		6 & 10	2.66				
	G8-H80		8 & 10	3.55				
Reference group	S6-H60	Steel bars	6 & 10					
	GS6-H60	GFRP & Steel bars	3ϕ10 GFRP bars & 3ϕ10 steel bars	2.66	GFRP hoops	ϕ6	60	1.65

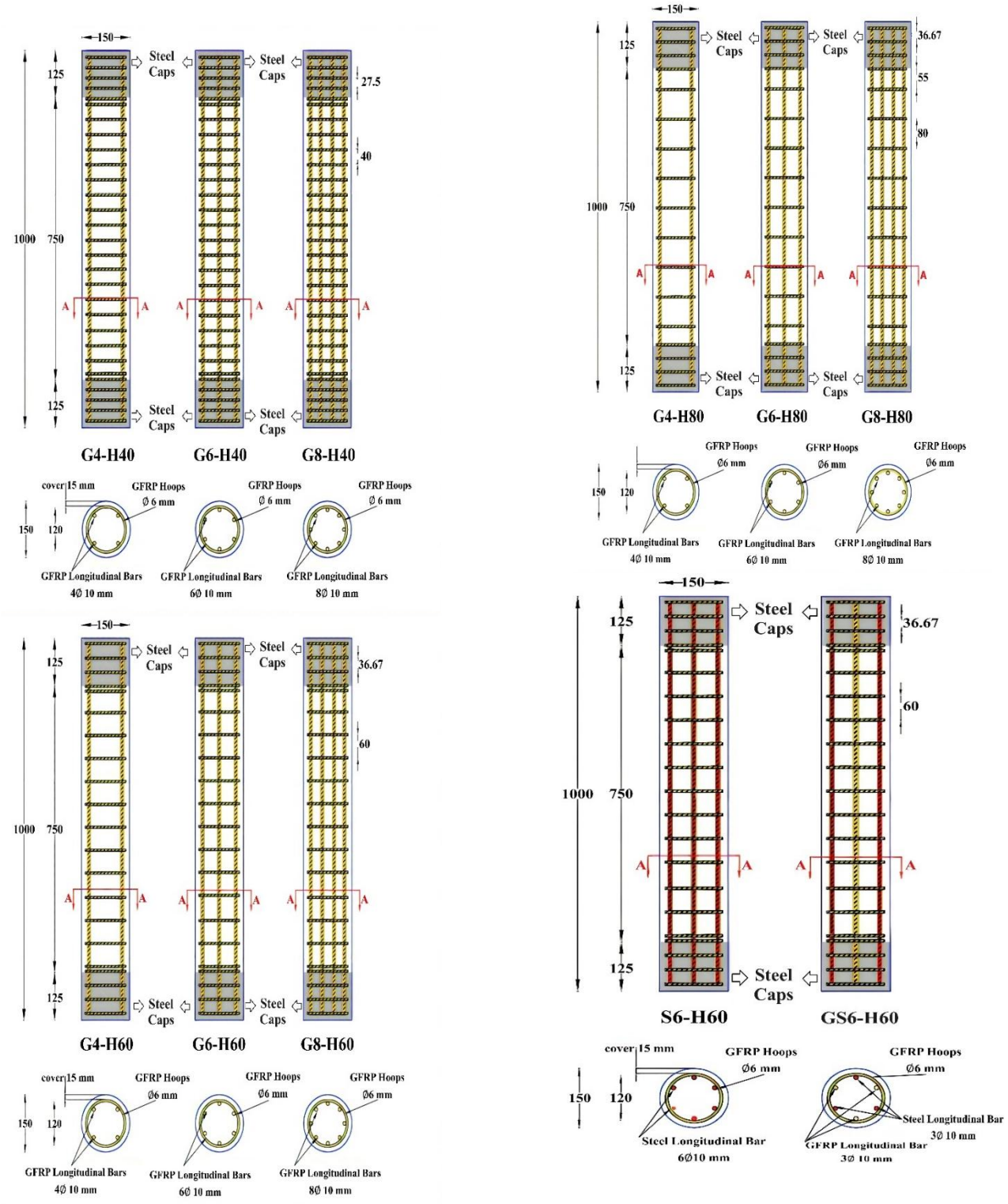

Figure 4. Configuration of reinforcement and geometric properties of the specimens.

All columns were designed according to ACI 440-22 [11] and CAN/CSA S807-19 [9] design standards. Columns were cast in a vertical orientation to replicate standard site practices, with the concrete placed in three approximately uniform concrete lifts to ensure uniform compaction and material distribution.

2.2 Test Setup and Instrumentation.

Four strain gauges were employed to monitor the strains in the enhancement throughout the experimental program. In addition, one strain gauge was attached to the concrete surface at the mid-height of each column along the axial axis to evaluate the concrete strain. The location of internal instrumentation is illustrated in Fig. 5. Moreover, column deformations in both

axial and lateral directions were recorded using a Linear Variable Differential Transformer (LVDT), as illustrated in Fig. 6. To avoid premature end failures caused by stress concentration and to ensure pin–pin boundary conditions, steel caps were installed at both ends of the specimens. These steel caps had an internal diameter of 150 mm and a thickness of 8 mm and were fixed over 125 mm lengths at the top and bottom of each column. Fig. 7 presents a representative schematic of the steel cap layout. Axial loading was applied using a 3000 kN universal testing machine and was increased gradually in steps of 10 kN until specimen failure. Throughout the testing process, the applied load and corresponding strains and displacements were continuously monitored and automatically recorded using a computerized data acquisition system. The standard test setup for concentrically loaded columns is illustrated in Fig. 8. In addition, a load cell was utilized to accurately measure the applied axial compressive force during testing. The load cell (Fig. 9) used was constructed from stainless steel with a capacity of 2000 kN, a combined error of 0.1 kN with the rate of loading. Moreover, the data logger KYOWA was used to read the deformations (strains and displacement) and load as shown in Fig. 10. The strain, displacement, and load readings were recorded using the latest version of the software program DIAdem (DIAdem 2022 Q4).

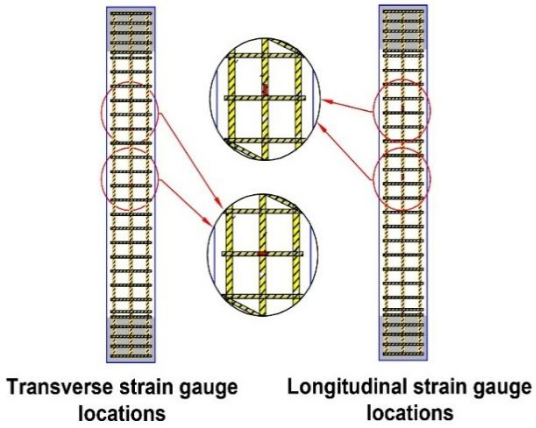

Figure 5. Location of internal strain gauges.

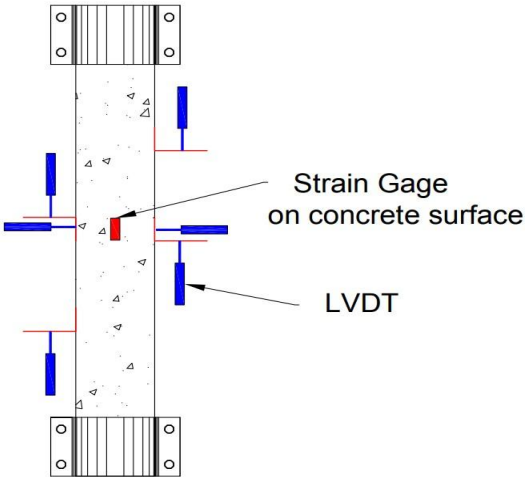

Figure 6. Position of external concrete strain gauges and LVDTs used to measure axial and lateral displacements.

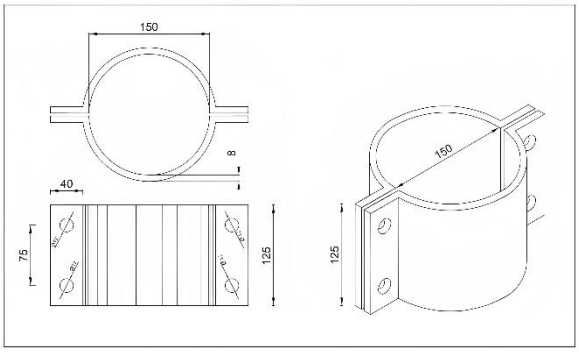

Figure 7. Layout and detailing of the steel cap.

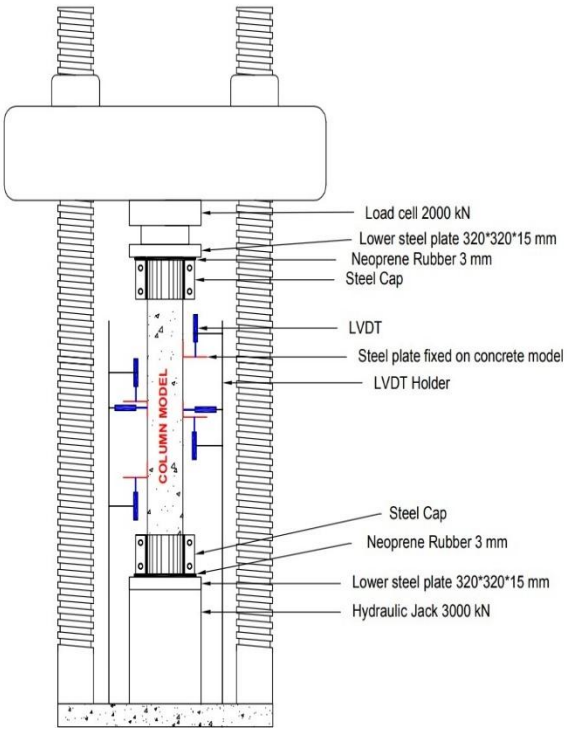

Figure 8. Schematic representation of the test setup.

Figure 9. Load cell.

Figure 10. Data logger connected to the computer PC.

3. Results and Discussions.

3.1 General Behavior and Failure Modes.

During experimental testing, the majority of the column specimens demonstrated comparable structural responses at different loading stages. The modes of failure of the specimens after the test are illustrated in Fig. 11. A sudden and unexpected catastrophic failure was observed in most specimens upon reaching the peak load. Unlike several concrete types reported in previous studies, the concrete and reinforcement systems adopted in this research did not exhibit visible cracking or progressive damage during the early and intermediate loading phases. However, as the applied load increased, partial spalling of the concrete cover was observed in some GFRP-RPC columns, particularly in specimens with relatively high load-bearing capacities. A distinctive phenomenon in GFRP-RPC specimens was the audible sound of reinforcement fracture prior to reaching peak load. This behavior may be attributed to the loss of bond between the reinforcement and concrete matrix, as well as internal rupture within the concrete core. The intensity of this sound increased as the applied load approached its maximum value. Following peak load, the load cell and testing machine detected a sudden decline in the recorded load. This drop was accompanied by rapid and violent deformation, resulting in sudden structural collapse. At failure, a loud noise was produced, and fragments of concrete were dispersed in multiple directions. The experimental findings are summarized in Table 6.

Analysis of the results indicates that the axial load capacity increased with higher longitudinal and transverse reinforcement ratios. Specimens containing greater reinforcement proportions exhibited more pronounced failure characteristics compared to those with lower reinforcement levels. In several columns, minor surface spalling occurred as a consequence of outward bulging and axial shortening caused by internal stress redistribution. Damage to the transverse GFRP hoops was generally less significant than that observed in the longitudinal GFRP bars, although deterioration became more evident at lower transverse reinforcement ratios. The optimal reinforcement configuration (Group G1) demonstrated the least structural damage. Within the reference specimens, the steel-reinforced column showed no damage to the GFRP hoops; however, buckling was detected in the steel bars. In contrast, the hybrid column exhibited rupture in one transverse hoop, buckling in all longitudinal steel bars, and fracture of all longitudinal GFRP bars.

a. First group (G1).

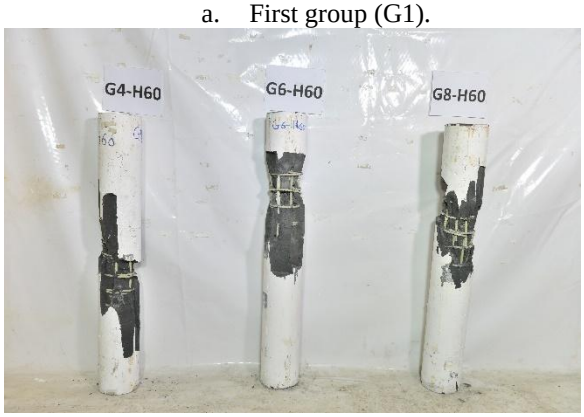

b. Second group (G2).

c. Third group (G3).

d. Fourth group (Reference Specimens).

Figure 11. Failure Mode of Tested Columns.

Table 6. The experimental test results

Group	ID specimens	Recorded Results at Maximum Load					
		Load (kN)	Displacement (mm)		Reinforcement Strains		Concrete Strains
		$P_{exp.}$ (kN)	δ_a (mm)	δ_l (mm)	ε_f (με)	ε_{hoop} (με)	ε_c (με)
G1	G4-H40	962.2	5.18	0.49	1968	255	1589
	G6-H40	1189.8	2.86	1.04	2250	288	1934
	G8-H40	1409.7	2.52	1.28	2477	326	2239
G2	G4-H60	910.5	3.96	1.20	1457	123	730
	G6-H60	1130.8	4.77	2.72	1322	141	656
	G8-H60	1328.3	4.30	2.91	1275	121	625
G3	G4-H80	875.4	4.48	1.48	1098	111	1048
	G6-H80	999	4.08	1.71	1198	134	1096
	G8-H80	1280.9	3.59	2.10	1371	101	1250
Ref.	S6-H60	1350.8	5.15	2.37	1673	113	894
	GS6-H60	1296.1	5.47	2.39	1615	250	571

* δ_a= axial displacement; δ_l= lateral displacement.

3.2 Load–Axial Displacement Response.

The relationship between axial load and axial displacement for tested columns is shown in Fig. 12. Axial shortening was recorded using four LVDTs, as previously indicated in Fig. 6. For the first specimen group, the maximum load obtained for columns G4-H40, G6-H40, and G8-H40 was 962.2 kN, 1189.8 kN, and 1409.7 kN, respectively. Compared with specimen G4-H40, these results correspond to load increases of approximately 23.7% for G6-H40 and 46.5% for G8-H40. The observed enhancement in load capacity is linked to the greater reinforcement ratios in both longitudinal and transverse directions, whereas the reduction in axial displacement is associated with the confining action of the GFRP hoops encasing the core. Subsequently, the longitudinal and GFRP hoop reinforcements failed, resulting in the ultimate failure of the columns, as depicted in Fig. 11. In addition, the recorded vertical displacements for columns G6-H40 and G8-H40 were 2.17 mm and 1.68 mm, respectively. These values indicate reductions of approximately 58.12% and 67.6% when compared to the vertical shortening of column G4-H40 under the same applied load of 962.2 kN. Regarding the second specimen group, the maximum axial loads obtained for columns G4-H60, G6-H60, and G8-H60 were 910.5 kN, 1130.8 kN, and 1328.3 kN, respectively. This corresponds to load increases of 24.2 and 45.9% for specimens G6-H60 and G8-H60, respectively, compared to G4-H60. Displacements at peak load: 3.96, 4.77, 4.30 mm. Moreover, the axial shortening measured for columns G6-H60 and G8-H60 was 3.51 mm and 3.38 mm, respectively. These values correspond to reductions of approximately 11.25% and 14.67% relative to the displacement recorded for column G4-H60 under the same loading condition of 910.5 kN. For the third specimen group, the maximum load capacities achieved by columns G4-H80, G6-H80, and G8-H80 were 875.4 kN, 999 kN, and 1280.9 kN, respectively. This represents load increases of 14.1 and 46.3% for specimens G6-H80 and G8-H80, respectively, compared to G4-H80. Displacements at peak load: 4.48, 4.08, 3.59 mm. In addition, the measured axial displacements of columns G6-H80 and G8-H80 were 3.02 mm and 1.72 mm, respectively. These results represent reductions of approximately 32.51% and 61.5% in comparison with the displacement recorded for column G4-H80 under the same applied load of 875.5 kN. With respect to the reference specimens, the maximum axial loads attained by columns S6-H60 and GS6-H60 were 1350.8 kN and 1296.1 kN, respectively. This represents load increases of 19.5 and 14.6%, respectively, compared to their counterparts in the GFRP-reinforced group, G6-H60. Displacements at peak load: 5.15, 5.47 mm. Additionally, the recorded vertical displacements for columns S6-H60 and GS6-H60 were 4.28 mm and 3.87 mm, respectively. These values correspond to reductions of approximately 10.31% and 18.78% when compared with the axial shortening of specimen G6-H60 under the same applied load of 1130.8 kN. Following the attainment of peak load, sudden and violent spalling of the concrete cover was observed in all columns, occurring without noticeable cracking. This phenomenon led to an abrupt and significant loss in load-carrying capacity. In addition, specimen S6-H60 showed an approximately linear ascending load behavior, followed by a linear descending load behavior after failure, with the load capacity continuing to decrease until the end of the test. Unlike all other specimens, specimen GS6-H60 exhibited two peak loads. The first peak load resulted from reaching the maximum compressive stress and the rupture of all bars of GFRP. Subsequently, there was a decrease in load, followed by a second peak load, characterized by the activation of the steel and its resistance to compression, before reaching the yield stress and then surpassing it after the failure occurred. Among

the GFRP-RPC specimens, column G4-H40 showed the largest vertical displacement at maximum load. The observed behavior resulted from the delayed confinement effect, attributed to the incremental approach of the transverse hoops before the specimen reached failure. Under these conditions, the longitudinal reinforcement was insufficient to effectively restrain the induced deformations, ultimately leading to rupture. In contrast, the G8-H40 exhibited higher stability and lower axial deformations than the other columns. Generally, the axial displacements were not excessively high, primarily due to the use of RPC composed of highly fine materials, which enhanced its ability to reduce axial deformations.

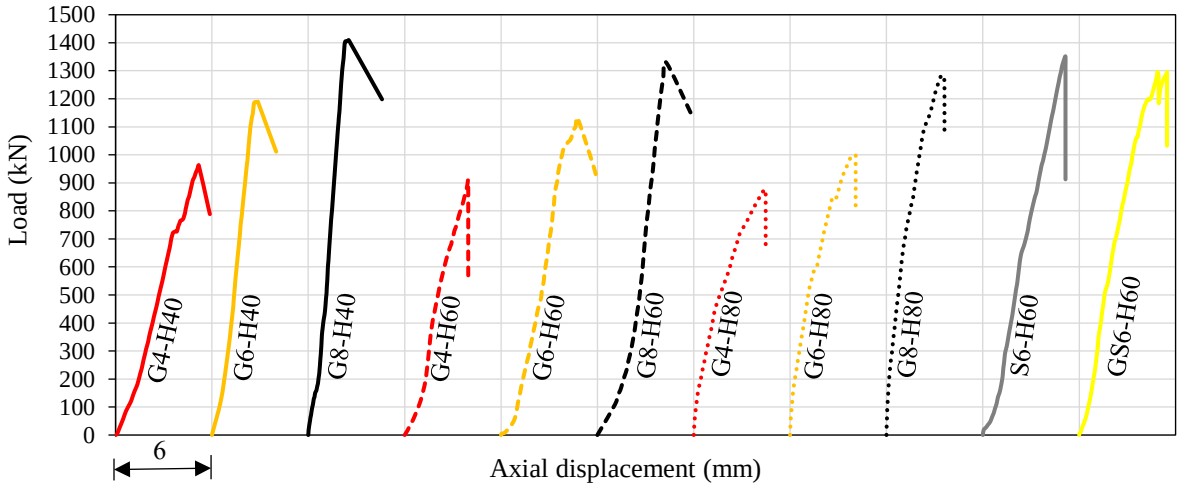

Figure 12. Relationship between applied load and axial displacement.

3.3 Longitudinal Compressive Strains (ε_f).

The relationships between the load and the axial compression strains in main bars are shown in Fig. 13. Initially, all columns exhibited similar behavior and showed a relatively ascending load-strain response until reaching the maximum load. The peak load and the corresponding longitudinal strain varied somewhat depending on the fundamental confinement characteristics. The longitudinal strains in GFRP bars at the maximum load (ε_f) are summarized in Table 6. Generally, closely spaced GFRP hoops enhance the (ε_f) for columns. The G8-H40 column showed the greatest (ε_f) data compared to columns, 2477 μ_ε, or 13.8% of the maximum tensile stress of GFRP reinforcements. The first group with 40 mm confinement showed that G6-H40 and G8-H40 had axial strains of 1502 and 1397 μ_ε, which are 23.7% and 29% lower than that of G4-H40 under 962.2 kN. Under an identical load of 910.5 kN, the specimens with moderate confinement (60 mm) exhibited notable differences in axial strain compared to G4-H60. Specifically, the axial strain for G6-H60 was 1243 μ_ε (a 14.7% decrease), While G8-H60 recorded a strain of 1006 μ_ε (a 31% decrease). In the small confinement group (80 mm), specimens G6-H80 and G8-H80 registered axial strains of 1054 and 927 μ_ε. These results were 3.96% and 15.54% lower, respectively, than the strain observed in the G4-H80 specimen at the same 875.4 kN loading. At the peak load (1350.8 kN), the Steel-RPC specimen's axial strain was 1673 μ_ε, representing 74.4% of the yield strain (2250 μ_ε). After peak load and before reaching 20% of the reduced load, the longitudinal strain of S6-H60 exceeded the yield strain. At the same loading level (1130.8 kN), the longitudinal strain data for reference specimens S6-H60 and GS6-H60 were 1256 and 1257 μ_ε, respectively, with a close decrease rate of 5% and 4.95% compared to their counterparts in the GFRP-RPC specimen (G6-H60).

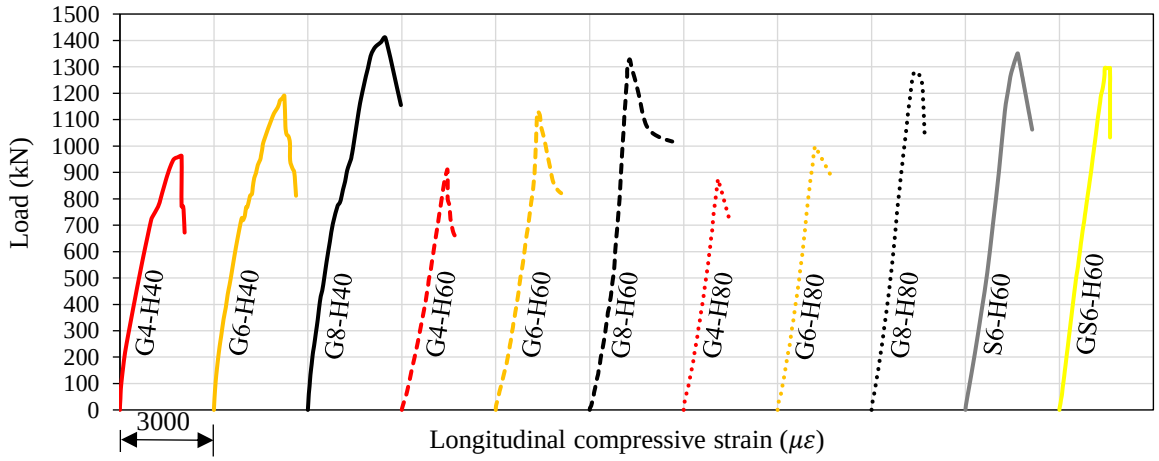

Figure 13. Load versus longitudinal compressive strain curves.

3.4 Ductility Index and Bar Contributions.

Ductility in reinforced concrete columns refers to their capacity to undergo large deformations and dissipate energy after reaching the ultimate axial load. This behavior can be assessed through parameters such as strain and deflection. Accordingly, the ductility index (D.I) was calculated using Equation (1) [29]-[31]:

$$D.I = \frac{A_{\delta 85}}{A_{\delta 75}} \quad (1)$$

As illustrated graphically in Fig. 14, the ductility index is derived from two distinct areas under the load-displacement curve. The area designated $A_{\delta 75}$ (area ABC) corresponds to the energy absorbed in the elastic region, measured up to the displacement (δ_{75}) at 75% of the ultimate axial load. The second area, $A_{\delta 85}$ (area ADE), represents the energy in the post-peak phase, measured up to the displacement (δ_{85}) at 85% of the ultimate load. The final calculated values for this ductility index across all tested columns are systematically organized in Table 7.

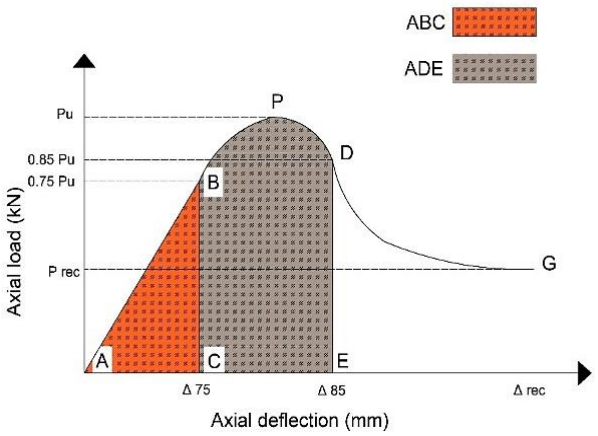

Figure 14. Plot showing the ductility index [29].

Table 7. The ductility index and bar contributions of all tested columns

Group	ID specimen	Measured Results at Peak Load			$\frac{A_{\delta 85}}{A_{\delta 75}}$)
		Load (kN)	Bar Contribution		
		$P_{exp.}$ (kN)	P_{bar} (kN)	$\frac{P_{bar}}{P_{exp.}}$ (%)	
G1	G4-H40	962.2	26	2.7	١,٨٣
	G6-H40	1189.8	44	3.7	٢,٢١
	G8-H40	1409.7	65	4.6	٢,٨٩
G2	G4-H60	910.5	19	2.1	١,٥٤
	G6-H60	1130.8	26	2.3	١,٩٦
	G8-H60	1328.3	33	2.5	٢,٤٤
G3	G4-H80	875.4	14	1.6	١,٣٠
	G6-H80	999	24	2.4	١,٦٧
	G8-H80	1280.9	36	2.8	٢,١٠
Ref.	S6-H60	1350.8	158	11.7	١,٥٠
	GS6-H60	1296.1	16 **	1.2	١,٦٣

* $P_{bar}=\varepsilon_f \times A_b \times E_f$; ε_f longitudinal strain that the GFRP bars bear at the ultimate load capacity (μ_ε); A_b the total area of the main bars (mm^2); E_f modulus of elasticity of longitudinal GFRP bars (MPa).

** For GFRP bars.

The initial response of the GFRP-RPC columns was predominantly brittle; however, this brittleness diminished with increases in both longitudinal and transverse reinforcement. Notably, specimens G6-H40, G8-H40, G8-H60, and G8-H80 exhibited higher ductility indices compared to the other specimens. Within the GFRP-RPC group, enhancing the lateral reinforcement ratio from 1.24 to 1.65 and 2.48 resulted in an increase in the ductility index of approximately 17.3% and 36.9%, respectively. So, reducing transverse reinforcement spacing leads to an increase in D.I. and ultimate axial strength in the confined section. Similarly, increasing the longitudinal reinforcement ratio from 1.77 to 2.66 and 3.55 increases the D.I by 25.5 and 59.3%, respectively. Additionally, the G4-H80 column got the lowest D.I value, while the G8-H40 specimen had the highest value of D.I. The results indicate that raising the main reinforcement ratio has a more pronounced impact on the ductility of the columns compared to the transverse reinforcement ratio. When compared with the reference specimens, the GFRP-RPC column exhibited a higher ductility index (1.96) than the Steel-RPC column (1.5). This difference is attributed to the fact that the steel bars in the Steel-RPC specimen did not undergo yielding, and therefore, the specimen did not achieve a comparable level of ductility. Furthermore, the GS6-H60 column exhibited a ductility index of 1.63, lower than that of the G6-H60 column (1.96) yet higher than the Steel-RPC column (1.5). This outcome supports the earlier observations and highlights a unique mechanism in the hybrid system, where the steel bars in the Hybrid-RPC column yielded immediately prior to the second peak load, unlike those in the Steel-RPC specimen, which remained unyielded. On the other hand, the contribution of GFRP bars is defined as the percentage of the load capacity of GFRP bars to the ultimate load capacity of the specimen ($P_{bar}/P_{exp.}$). P_{bar} depends on the strain values of the longitudinal GFRP bars, recorded at ultimate load capacity, and on the elasticity modulus of these bars reported by the manufacturer. The benefit of calculating the contribution of the bars is to determine and evaluate the ultimate contributions of GFRP bars to the ultimate load capacity of the column. The bar contribution of GFRP bars for GFRP-RPC columns ranges from 1.6 to 4.6%. In addition, raising the main enhancement ratio from 1.77% to 2.66% resulted in a bar contribution ranging from 2.3% to 3.7%. Furthermore, raising the main reinforcement ratio from 1.77% to 3.55% led to a bar contribution ranging from 2.5% to 4.6%. So, the contribution of GFRP bars is closely related to the longitudinal reinforcement ratio of GFRP-RPC specimens, as illustrated in Fig. 15.

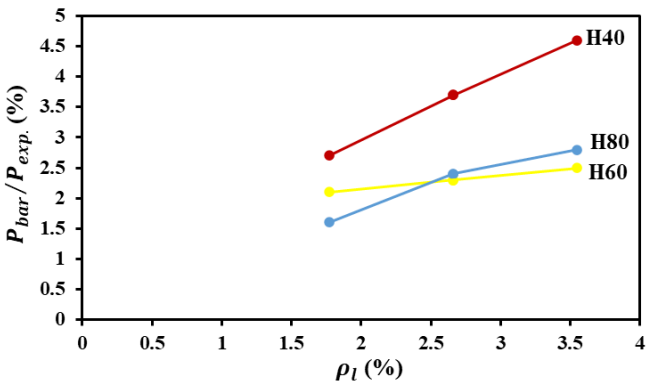

Figure 15. Contribution of GFRP bars to load capacity for GFRP-RPC specimens ($P_{bar}/P_{exp.}$) vs. longitudinal reinforcement ratio (ρ_l) curve.

For the reference specimens, the steel bars' contribution for specimen S6-H60 was 11.7% of the ultimate load, while in specimen GS6-H60, the contribution of GFRP and Steel bars was 1.2 and 8.18%, respectively. This behavior was expected since the elasticity modulus of steel is higher than that of GFRP, making Steel-RPC and Hybrid-RPC columns have a higher longitudinal bar contribution to ultimate load.

3.5 Effect of Longitudinal Reinforcement Ratio.

The design of the GFRP-RPC columns was guided by ACI 440-22 [10], which specifies an allowable range for the longitudinal reinforcement ratio of 1% to 8% for GFRP-reinforced concrete columns. Based on this, three different ratios were selected for the design: 1.77%, 2.66%, and 3.55% (detailed in Table 5). It was observed that lower reinforcement ratios led to brittle failure modes with limited ductility. In contrast, columns with higher ratios (2.66% and 3.55%) behaved more favorably. Specifically, an increase in the main reinforcement from 1.77% to 2.66% yielded a corresponding rise in axial load capacity, ranging from 14.12% to 24.2%. A more significant improvement was noted when the ratio was increased from 1.77% to 3.55%, which resulted in an approximate 46% gain in axial load. Fig. 16 visually represents the effect of the main reinforcement ratio on the ultimate load capacity of the GFRP-RPC columns.

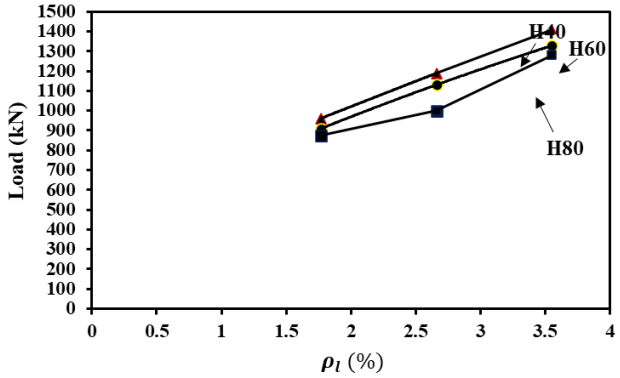

Figure 16. Influence of ρ_l on ultimate load for GFRP-RPC columns.

The presented results clearly demonstrate that raising the main reinforcement ratio substantially improves the load-carrying capacity of the columns. After peak load, the GFRP-RPC specimens experienced a substantial reduction in ultimate capacity, resulting from concrete cover crushing and the rupture or buckling of most primary reinforcement bars. Post-peak curves rapidly declined in strength, but readings were safely recorded until test termination. Finally, the similarities between the current study and previous studies highlight the importance of studying the effect of longitudinal reinforcement ratio on the behavior of columns reinforced with GFRP bars.

3.6 Effect of Transverse Reinforcement Ratio.

The allowable transverse reinforcement ratio for reinforced concrete columns with GFRP bars according to ACI 440-22 [11] ranges from 1% to 8%. Based on this, GFRP-RPC columns were designed. The specimens were designed with three different transverse reinforcement ratios for each group (2.48 %, 1.65 %, and 1.24 %, respectively), as previously detailed in Table 5. Specimens with a low transverse reinforcement ratio (1.24%) exhibited brittle and sudden failure compared to those with higher ratios (1.65% and 2.48%). A 3.7% to 13.19% increase in axial load was achieved in GFRP-RPC samples by raising the lateral reinforcement ratio from 1.24% to 1.65%. Further raising of the ratio from 1.24% to 2.48% led to a rise in axial load ranging from about 9.91% to 19.1%. The impact of the lateral enhancement ratio on the peak load of the GFRP-RPC samples is presented in Fig. 17.

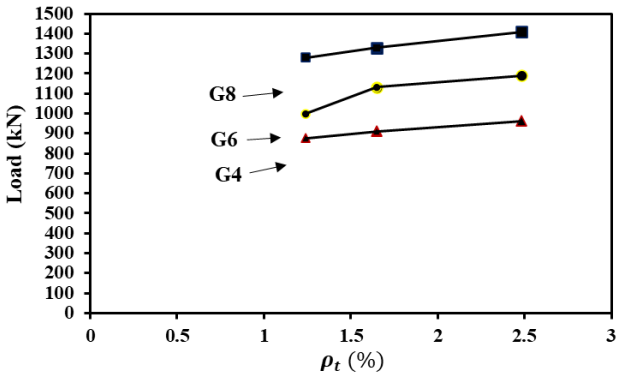

Figure 17. Influence of ρ_t on ultimate load for GFRP-RPC specimens.

The previous results indicate that increasing the transverse reinforcement ratio markedly improves the load-carrying capacity of the columns. Specimens reinforced transversely at 2.48% exhibited a favorable failure behavior, preserving the concrete core while the surrounding cover concrete crushed. Specimens reinforced transversely at 1.24% experienced brittle failure with limited warning, characterized by concrete cover crushing and lateral reinforcement rupture, even under a high longitudinal reinforcement ratio. Additionally, higher transverse reinforcement ratios appeared to mitigate twisting in the longitudinal GFRP bars to some extent.

3.7. Effect of the Types of Longitudinal Reinforcement.

As mentioned earlier, the allowable longitudinal reinforcement ratio for reinforced concrete columns with GFRP bars

according to ACI 440-22 [11] ranges from 1% to 8%. Based on this, GFRP-RPC columns were designed. Regarding the reference specimens, a Steel-RPC specimen was designed in accordance with ACI 318-19 [32], which ranged from 1% to 8%. As for the Hybrid RPC specimen, it was designed with a similar ratio to the GFRP-RPC and Steel-RPC specimens as a case study. The influence of longitudinal reinforcement type can be obtained from the specimen results (G6-H60, S6-H60, and GS6-H60). All three specimens had a longitudinal reinforcement ratio of 2.66% with a 60-mm spacing. The S6-H60 and GS6-H60 columns demonstrated increases in load capacity of approximately 19.45% and 14.61%, respectively, relative to the G6-H60 column. The effect of the type of longitudinal reinforcement on load versus axial displacements for the three specimens is illustrated in Fig. 18. The measured longitudinal deformation for columns S6-H60 and GS6-H60 was 4.28 mm and 3.87 mm, respectively. These values represent reductions of approximately 10.31% and 18.78% in comparison to the longitudinal deformation of column G6-H60, which was 4.77 mm under the same applied load of 1130.8 kN. Moreover, specimen S6-H60 showed an approximately linear ascending load behavior, followed by a linear descending load behavior after failure, with the load capacity continuing to decrease until the end of the test. The perfect ascending curve suggests that using GFRP hoops with longitudinal steel bars didn't adversely affect column behavior. The observed response resulted from the evolution and spread of stresses within the concrete core, accompanied by the widening interaction between reinforcement and concrete, which ultimately led to reinforcement buckling and sudden spalling of the concrete cover. Unlike all other specimens, specimen GS6-H60 exhibited two peak loads. The first peak load resulted from reaching the maximum compressive stress and the rupture of all bars of GFRP. Subsequently, there was a decrease in load, followed by a second peak load, characterized by the activation of the steel and its resistance to compression, before reaching the yield stress and then surpassing it after the failure occurred. In summary, the axial displacements were not excessively high, primarily due to the use of RPC composed of highly fine materials, which enhanced its ability to reduce axial deformations.

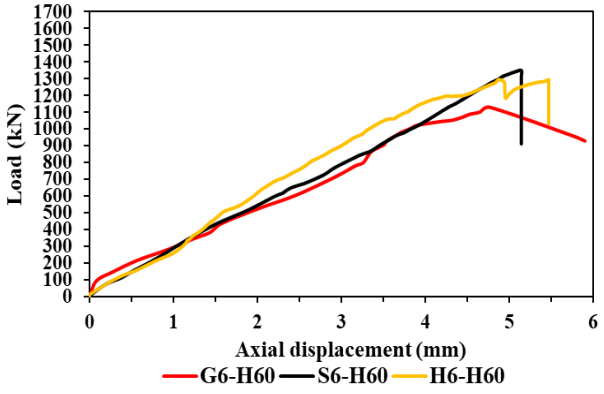

Figure 18. Influence of the type of longitudinal reinforcement on axial displacement.

The effect of the type of longitudinal reinforcement on load versus longitudinal compressive strains for the three specimens is illustrated in Fig. 19. The axial strains measured for columns S6-H60 and S6-H60 were 1255.9 μ_ε and 1256.6 μ_ε, respectively. These correspond to reductions of approximately 5% and 4.95% compared with the GFRP-RPC specimen G6-H60, which exhibited a longitudinal strain of 1322 μ_ε under the same applied load of 1130.8 kN. At the same load level of 1130.8 kN, the longitudinal strain in the steel bars of GS6-H60 (1478.6 μ_ε) was 11.85% greater than the axial strain of the G6-H60 column (1322 μ_ε). Conversely, it can be observed that the strain in G6-H60 was higher than that in S6-H60 and GS6-H60 at the same load level, attributed to the lower modulus of elasticity of GFRP bars compared to steel bars.

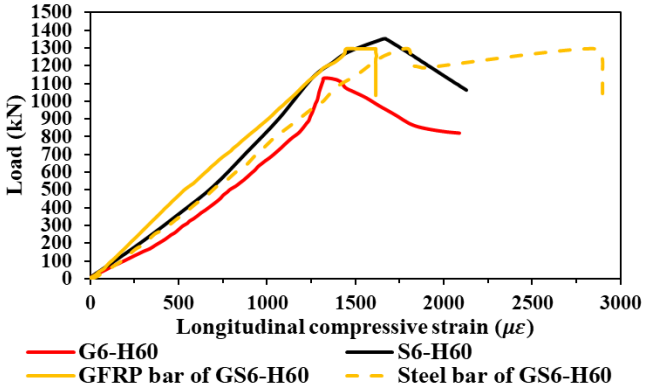

Figure 19. Influence of the type of longitudinal reinforcement on ε_f.

3.8 Design equation of GFRP-RC columns.

To evaluate the axial load of the GFRP-RC columns, a set of eleven analytical formulas was considered. These formulas, along with their formulations and respective references, are summarized in Table 8. For clarity, each model was assigned a unique identifier to facilitate comparison.

To assess the performance of each analytical model, the theoretical axial load was calculated and subsequently compared against its corresponding experimental counterpart. From the ratio of the experimental to the theoretical load, three principal statistical indicators were derived: the mean, the standard deviation (SD), and the coefficient of variation (COV). These statistical indicators function as metrics for gauging the precision and reliability of each equation. An equation yielding a mean close to one indicates better predictive capability, while a higher standard deviation reflects lower reliability due to greater data dispersion. Similarly, a lower COV implies higher consistency and improved predictive accuracy. Table 9 summarizes the ratios of experimental to theoretical load capacities for the GFRP-reinforced circular concrete columns. The data indicate that the ACI 440-22 and CSA S806-12 equations, both of which disregard the contribution of GFRP reinforcement, demonstrated significant variability. Specifically, the COV values were high, at 17.32% for ACI 440-22 and 17.99% for CSA S806-12, as were the SD values, which were recorded as 0.152 and 0.191, respectively. Their average ratios were 0.88 and 1.06, respectively.

Table 8. Summary of predictive models for axial load capacity

No.	Reference	Formulation	Parameter Definition
1	ACI 440-22 [11]	$P_o = \alpha_1 f'_c A_g$	α_1=0.85
2	CSA S807-19 [9]	$P_o = \alpha_1 f'_c (A_g - A_f) + f_{FRP} A_f$	α_1=0.85; f_{FRP}=0.002E_f
3	Hasan et al. [33]	$P_o = \alpha_1 f'_c (A_g - A_f) + \varepsilon_{co} E_f A_f$	α_1=0.85; ε_{co}= 0.0005$(f'_c)^{0.4}$
4	AS–3600 [34]	$P_o = \alpha_1 f'_c (A_g - A_f) + f_{FRP} A_f$	α_1=0.85; f_{FRP}=0.0025E_f
5	Hadhood et al. [35]	$P_o = \alpha_1 f'_c (A_g - A_f) + f_{FRP} A_f$	$\alpha_1 = 0.85 - 0.0015 f'_c$ f_{FRP}=0.0035E_f
6	Maranan et al. [36]	$P_o = \alpha_1 f'_c (A_g - A_f) + f_{FRP} A_f$	α_1=0.9; f_{FRP}=0.002E_f
7	Hadi et al. [37]	$P_o = \alpha_1 f'_c (A_g - A_f) + \varepsilon_f E_f A_f$	α_1=0.85; ε_f=0.003
8	Mohamed et al. [2]	$P_o = \alpha_1 f'_c (A_g - A_f) + \varepsilon_f E_f A_f$	α_1=0.85; ε_f=0.002
9	Afifi et al. [38]	$P_o = \alpha_1 f'_c (A_g - A_f) + \alpha_f f_{fu} A_f$	α_1=0.85; α_f=0.35
10	Tobbi et al. [39]	$P_o = \alpha_1 f'_c (A_g - A_f) + \alpha_f f_{fu} A_f$	α_1=0.85; α_f=0.35
11	CAN/CSA S806-12 [8]	$P_o = \alpha_1 f'_c (A_g - A_f)$	$\alpha_1 = 0.85 - 0.0015 f'_c \geq 0.67$

* The value of ε_{co}In Hasan et al.'s equation was determined using a formulation proposed by Leggeron and Poulter [40], which has been shown to provide good agreement with the experimentally measured values.

On the whole, the equations that incorporated the elastic modulus of the GFRP bars into their framework demonstrated lower SD and COV values when contrasted with models that were dependent on the axial strain of the primary reinforcing bars, such as the approach by Hadi and Mohamed, including approaches where the GFRP axial strain was assumed equal to the concrete strain at peak stress (Mohamed). Among all models, Hadhood's equation provided the optimal mean value, while other models—ACI 440-22, CSA S807-19, Hasan, AS–3600, Hadi, and Mohamed—produced mean ratios ranging from 0.86 to 0.88. Equations by Maranan, Afifi, and Tobbi showed slightly lower mean values between 0.82 and 0.84. Despite having a mean of 0.82, Tobbi's equation was considered relatively more reliable due to its lower SD and COV. In summary, equations incorporating the elasticity modulus of GFRP bars in the calculation of axial load capacity for reinforced concrete columns offer relatively higher reliability, reduced dispersion, and acceptable safety compared to other models.

Table 9. Comparison between measured and predicted axial capacities of circular GFRP-RC columns

No.	ID columns	$P_{exp.}/P_o$ Equation number										
		1	2	3	4	5	6	7	8	9	10	11
1	G4-H40	0.75	0.75	0.74	0.75	0.86	0.71	0.74	0.75	0.73	0.72	0.90
2	G6-H40	0.93	0.93	0.91	0.92	1.05	0.88	0.91	0.93	0.89	0.87	1.12
3	G8-H40	1.10	1.09	1.07	1.08	1.23	1.04	1.07	1.09	1.04	1.01	1.34
4	G4-H60	0.71	0.71	0.70	0.71	0.82	0.67	0.70	0.71	0.69	0.68	0.85
5	G6-H60	0.89	0.88	0.87	0.87	1.00	0.83	0.87	0.88	0.85	0.83	1.07
6	G8-H60	1.04	1.03	1.01	1.02	1.16	0.98	1.01	1.03	0.98	0.95	1.26
7	G4-H80	0.69	0.68	0.68	0.68	0.79	0.65	0.68	0.68	0.67	0.65	0.82
8	G6-H80	0.78	0.78	0.77	0.77	0.89	0.74	0.77	0.78	0.75	0.73	0.94
9	G8-H80	1.00	0.99	0.98	0.98	1.12	0.94	0.97	0.99	0.95	0.91	1.22
Avg.		0.88	0.87	0.86	0.86	0.99	0.82	0.86	0.87	0.84	0.82	1.06
SD		0.152	0.149	0.144	0.147	0.162	0.142	0.144	0.149	0.136	0.127	0.191
COV (%)		17.32	17.14	16.76	16.94	16.30	17.19	16.74	17.14	16.16	15.50	17.99

4. Conclusions.

The study investigates GFRP-RPC columns' behavior under axial load. Eleven specimens were tested according to longitudinal reinforcement ratio, hoop spacing, and longitudinal type effect. Key findings:

- Increasing longitudinal reinforcement ratio increases GFRP-RPC column capacity (21-46%).
- The transverse reinforcement ratio controls the failure mode, with failure being rather ductile with a ratio equal to 2.48% and brittle and explosive at other ratios (1.65 and 1.24%).
- Transverse reinforcement contributes more as longitudinal reinforcement decreases.
- The increasing transverse reinforcement ratio improves the ductility, as it reached an average of 2.31 for the group with a ratio of 2.48%, while it was 1.98 and 1.69 for the groups with 1.65% and 1.24%, respectively.
- GFRP-RPC ductility is higher than that of Steel-RPC and Hybrid-RPC.
- GFRP-RPC and Steel-RPC columns exhibited similar behaviour in terms of failure mode and linear load-compressive strain response.
- The rupture of GFRP bars and hoops dominated the failure mode of GFRP-RPC columns, accompanied by concrete crushing and spalling, while the buckling of steel bars and the rupturing of GFRP hoops controlled the failure mode of Steel-RPC, accompanied by concrete crushing.
- GFRP hoops confine concrete even post-failure.
- GFRP-RPC capacity is slightly lower than Steel-RPC and Hybrid-RPC.
- The available equations for calculating the load capacity of RC columns with GFRP bars show that equations based on the modulus of elasticity of these reinforcements provide more reliable estimations than equations relying on axial strains at the peak load, despite some of them yielding a somewhat conservative average. However, it might be appropriate to use them if a reasonable safety factor is provided during the design process.

Finally, GFRP reinforcement is viable for columns, preserving durability. Further study is needed for other loading conditions and FRP types.

Acknowledgements.

This scientific paper is part of an M.Sc. thesis at the Civil Engineering Department, College of Engineering, Mustansiriyah University, and the authors express their sincere thanks and gratitude to the Journal of Engineering and Sustainable Development (JEASD) for the support provided.

Abbreviations.

ε_f	Axial strain that the GFRP bars bear at the maximum load capacity (μ_ε)
f'_c	Compressive strength of the concrete (MPa)
ε_{co}	Concrete strain (μ_ε)
ρ_l	Longitudinal reinforcement ratio (%)
f_{frp}	Multiplying of the maximum axial strain that the GFRP bars bear at the maximum load capacity by the modulus of elasticity of the GFRP bars
E_f	Stiffness (modulus of elasticity) of GFRP bars (MPa)
f_{fu}	Tensile strength of the GFRP bars (MPa)
A_f	Total cross-section area of GFRP bars (mm^2)
ρ_t	Transverse reinforcement ratio (%)

Conflict of interest.

The authors declare that there are no conflicts of interest regarding the publication of this manuscript.

Author Contribution Statement

Mohamed Qassim Kadhim verified the analytical methods and investigated practically the behavior of concentrically loaded RPC circular columns reinforced longitudinally and transversally with GFRP bars. Hassan Falah Hassan proposed the research problem and supervised the research. Results and contributions to the final manuscript were discussed by Mohamed Qassim Kadhim.

References.

[1] Z. F. Yawer and A. H. Aziz, "Performance of corroded thin-walled steel tubular columns filled with concrete under direct monotonic loading," *Journal of Engineering and Sustainable Development*, vol. 27, no. 2, pp. 213–226, 2023. doi: https://doi.org/10.31272/jeasd.27.2.6

[2] H. M. Mohamed, M. Z. Afifi, and B. Benmokrane, "Performance evaluation of concrete columns reinforced longitudinally with FRP bars and confined with FRP hoops and spirals under axial load," *Journal of Bridge Engineering*, vol. 19, no. 7, pp. 04014020, 2014. doi: https://doi.org/10.1061/(ASCE)BE.1943-5592.0000590

[3] E. Alrehaili, A. Nurdiawati, and S. G. Al-Ghamdi, "Sustainable Composites for Metal Replacement: Environmental Assessment and Material Selection of Fiber-Reinforced Polymer across Industries," *Resources Conservation & Recycling Advances*, vol. 28, pp. 200294–200294, Oct. 2025, doi: https://doi.org/10.1016/j.rcradv.2025.200294

[4] *ACI Committee 440*, **ACI 440.1R-15**, *Guide for the Design and Construction of Structural Concrete Reinforced with FRP Bars*, American Concrete Institute, Farmington Hills, MI, USA, 2015.

[5] H. M. Mohamed and B. Benmokrane, "Design and performance of reinforced concrete water chlorination tank totally reinforced with GFRP bars: Case study," *Journal of Composites for Construction*, vol. 18, no. 1, pp. 05013001, 2014. doi: https://doi.org/10.1061/(ASCE)CC.1943-5614.0000429

[6] R. Z. Hamed and H. F. Hassan, "Structural behavior of GFRP-RC slender columns under various eccentricity loading conditions," *Civil and*

Environmental Engineering Reports, vol. 19, no. 1, pp. 1–16, 2023. doi: https://doi.org/10.2478/cee-2023-0001

[7] P. Wang, W. Hao, L. Ke, W. Li, and C. F. Leung, "Mechanical Properties and Microstructure of Glass Fiber Reinforced Polymer (GFRP) Rebars Embedded in Carbonated Reactive MgO-based Concrete (RMC)," *Cement and Concrete Composites*, vol. 142, pp. 105207–105207, Sep. 2023, doi: https://doi.org/10.1016/j.cemconcomp.2023.105207

[8] CSA Group, **CAN/CSA S806-12 (R2017)**, *Design and Construction of Building Structures with Fibre-Reinforced Polymers*, Canadian Standards Association, Mississauga, ON, Canada, 2012 (reaffirmed 2017).

[9] CSA Group, **CSA S807-19**, *Specification for Fibre-Reinforced Polymers*, Canadian Standards Association, Toronto, ON, Canada, 2019.

[10] ACI Committee 440, **ACI 440.1R-06**, *Guide for the Design and Construction of Structural Concrete Reinforced with FRP Bars*, American Concrete Institute, Farmington Hills, MI, USA, 2006.

[11] ACI Committee 440, **ACI 440.11-22**, *Building Code Requirements for Structural Concrete Reinforced with Glass Fiber-Reinforced Polymer (GFRP) Bars—Code and Commentary*, American Concrete Institute, Farmington Hills, MI, USA, 2022.

[12] P. Richard and M. Cheyrezy, "Composition of reactive powder concretes," *Cement and Concrete Research*, vol. 25, no. 7, pp. 1501–1511, 1995. doi: https://doi.org/10.1016/0008-8846(95)00144-2

[13] H. Li, F. Wu, L. Bu, Y. Liu, and J. Yao, "Study on the compression performance of steel reactive powder concrete columns," *Advances in Structural Engineering*, vol. 23, no. 10, pp. 2018–2029, 2020. doi: https://doi.org/10.1177/1369433220903986

[14] A. H. Mohammed, L. A. G. Yassin, and M. M. Hamid, "Experimental investigation on the ultimate capacity of rectangular reinforced hybrid concrete columns under axial load," *GEOMATE Journal*, vol. 23, no. 95, pp. 112–118, 2022. doi: https://doi.org/10.21660/2022.95.3210

[15] L. Zhang, M. Zhang, K. Wang, J. Shi, W. Chen, and K. Yan, "Axial compressive behavior of steel-reinforced reactive powder concrete short columns," *Structures*, vol. 46, pp. 433–444, 2022. doi: https://doi.org/10.1016/j.istruc.2022.10.073

[16] M. N. Hadi, H. A. Hasan, and M. N. Sheikh, "Experimental investigation of circular high-strength concrete columns reinforced with glass fiber-reinforced polymer bars and helices under different loading conditions," *Journal of Composites for Construction*, vol. 21, no. 4, pp. 04017005, 2017. doi: https://doi.org/10.1061/(ASCE)CC.1943-5614.0000784

[17] N. P. Duy, V. N. Anh, N. Minh, T. Anh, and P. A. Eduardovich, "Load-carrying capacity of short concrete columns reinforced with glass fiber reinforced polymer bars under concentric axial load," *International Journal of Engineering and Advanced Technology*, vol. 9, no. 2, pp. 1712–1719, 2019. doi: https://doi.org/10.35940/ijeat.b2372.129219

[18] S. El Gamal and O. Alshareedah, "Experimental study on the performance of circular concrete columns reinforced with GFRP under axial load," in *International Conference on Civil Infrastructure and Construction (CIC 2020)*, Doha, Qatar, 2020. doi: https://doi.org/10.29117/cic.2020.0115

[19] M. Elchalakani, T. Aly, and W. Nawaz, "Behavior of circular concrete columns reinforced with GFRP bars and spirals under axial and eccentric loading," in *Concrete Institute of Australia's 30th National Conference 2021*, Perth, Australia, 2021. [Online]. Available: https://www.researchgate.net/publication/358886056_Behavior_of_Circular_concrete_columns_reinforced_with_GFRP_bars_and_spirals_under_axial_and_eccentric_loading

[20] M. G. Gouda, H. M. Mohamed, A. C. Manalo, and B. Benmokrane, "Behavior of hollow glass fiber-reinforced polymer-reinforced concrete columns under axial load: Experimental and theoretical investigation," *ACI Structural Journal*, vol. 119, no. 6, pp. 289–302, 2022. doi: https://doi.org/10.14359/51736117

[21] Central Organization for Standardization and Quality Control (COSQC), **IQS No. 45/1984**, *Aggregate from Natural Sources for Concrete and Construction*, Ministry of Planning, Baghdad, Iraq, 1984.

[22] H. F. Hassan, "Punching shear behavior of normal and modified reactive powder concretes slabs," Ph.D. dissertation, Civil Engineering Dept., Mustansiriyah University, Baghdad, Iraq, 2012.

[23] ASTM International, **ASTM C109/C109M-21**, *Standard test method for compressive strength of hydraulic cement mortars*, West Conshohocken, PA, USA, 2021. doi: https://doi.org/10.1520/C0109_C0109M-21

[24] ASTM International, **ASTM C1437-20**, *Standard test method for flow of hydraulic cement mortar*, West Conshohocken, PA, USA, 2020. doi: https://doi.org/10.1520/C1437-20

[25] ASTM International, **ASTM C39/C39M-21**, *Standard test method for compressive strength of cylindrical concrete specimens*, West Conshohocken, PA, USA, 2021. doi: https://doi.org/10.1520/C0039_C0039M-21

[26] ASTM International, **ASTM C496/C496M-17**, *Standard test method for splitting tensile strength of cylindrical concrete specimens*, West Conshohocken, PA, USA, 2017. doi: https://doi.org/10.1520/C0496_C0496M-17

[27] ASTM International, **ASTM D7205/D7205M-21**, *Standard test method for tensile properties of fiber reinforced polymer matrix composite bars*, West Conshohocken, PA, USA, 2021. doi: https://doi.org/10.1520/D7205_D7205M-21

[28] ASTM International, **ASTM A615/A615M-22**, *Standard specification for deformed and plain carbon-steel bars for concrete reinforcement*, West Conshohocken, PA, USA, 2022. doi: https://doi.org/10.1520/A0615_A0615M-22

[29] A. Raza and A. Ahmad, "Investigation of HFRC columns reinforced with GFRP bars and spirals under concentric and eccentric loadings," *Engineering Structures*, vol. 227, pp. 111461, 2021. doi: https://doi.org/10.1016/j.engstruct.2020.111461

[30] M. Elchalakani and G. Ma, "Tests of glass fibre reinforced polymer rectangular concrete columns subjected to concentric and eccentric axial loading," *Engineering Structures*, vol. 151, pp. 93–104, 2017. doi: https://doi.org/10.1016/j.engstruct.2017.08.023

[31] M. Elchalakani, M. Dong, A. Karrech, G. Li, M. S. Mohamed Ali, and B. Yang, "Experimental investigation of rectangular air-cured geopolymer concrete columns reinforced with GFRP bars and stirrups," *Journal of Composites for Construction*, vol. 23, no. 3, pp. 04019011, 2019. doi: https://doi.org/10.1061/(ASCE)CC.1943-5614.0000938

[32] ACI Committee 318, **ACI 318-19**, *Building code requirements for structural concrete (ACI 318-19) and commentary (ACI 318R-19)*, American Concrete Institute, Farmington Hills, MI, USA, 2019.

[33] H. A. Hasan, M. N. Sheikh, and M. N. Hadi, "Maximum axial load carrying capacity of fibre reinforced-polymer (FRP) bar reinforced concrete columns under axial compression," *Structures*, vol. 19, pp. 227–233, 2019. doi: https://doi.org/10.1016/j.istruc.2019.02.008

[34] Standards Australia, **AS 3600:2018**, *Concrete structures*, Sydney, Australia, 2018.

[35] A. Hadhood, H. M. Mohamed, and B. Benmokrane, "Strength of circular HSC columns reinforced internally with carbon-fiber-reinforced polymer bars under axial and eccentric loads," *Construction and Building Materials*, vol. 141, pp. 366–378, 2017. doi: https://doi.org/10.1016/j.conbuildmat.2017.02.117

[36] G. B. Maranan, A. C. Manalo, B. Benmokrane, W. Karunasena, and P. Mendis, "Behavior of concentrically loaded geopolymer-concrete circular columns reinforced longitudinally and transversely with GFRP bars," *Engineering Structures*, vol. 117, pp. 422–436, 2016. doi: https://doi.org/10.1016/j.engstruct.2016.03.036

[37] M. N. Hadi, H. Karim, and M. N. Sheikh, "Experimental investigations on circular concrete columns reinforced with GFRP bars and helices under different loading conditions," *Journal of Composites for Construction*, vol.

20, no. 4, pp. 04016009, 2016. doi: https://doi.org/10.1061/(ASCE)CC.1943-5614.0000670

[38] M. Z. Afifi, H. M. Mohamed, and B. Benmokrane, "Strength and axial behavior of circular concrete columns reinforced with CFRP bars and spirals," *Journal of Composites for Construction*, vol. 18, no. 2, pp. 04013035, 2014. doi: https://doi.org/10.1061/(ASCE)CC.1943-5614.0000430

[39] H. Tobbi, A. S. Farghaly, and B. Benmokrane, "Concrete columns reinforced longitudinally and transversally with glass fiber-reinforced polymer bars," *ACI Structural Journal*, vol. 109, no. 4, pp. 551–558, 2012. doi: https://doi.org/10.14359/51683874

[40] F. Légeron and P. Paultre, "Uniaxial confinement model for normal- and high-strength concrete columns," *Journal of Structural Engineering*, vol. 129, no. 2, pp. 241–252, 2003. doi: https://doi.org/10.1061/(ASCE)0733-9445(2003)129:2(241)